Small-Angle Neutron Scattering (SANS) Study of Vesicles and Lamellar Sheets Formed from Mixtures of an Anionic and a Cationic Surfactant

ARTICLE *in* THE JOURNAL OF PHYSICAL CHEMISTRY B · OCTOBER 1999

Impact Factor: 3.3 · DOI: 10.1021/jp991846w

2 AUTHORS:

Magnus Bergstrom
Uppsala University
62 PUBLICATIONS **1,568** CITATIONS
SEE PROFILE

Jan Skov Pedersen
Aarhus University
363 PUBLICATIONS **10,991** CITATIONS
SEE PROFILE

Small-Angle Neutron Scattering (SANS) Study of Vesicles and Lamellar Sheets Formed from Mixtures of an Anionic and a Cationic Surfactant

Magnus Bergström* and Jan Skov Pedersen

Condensed Matter Physics and Chemistry Department, Risø National Laboratory, DK-4000 Roskilde, Denmark

Peter Schurtenberger

Institut für Polymere, ETH Zürich, CH-8092 Zürich, Switzerland

Stefan U. Egelhaaf†

Institute Laue-Langevin, Large Scales Structure Group, B.P. 156, F-38042 Grenoble Cedex 9, France

Received: June 7, 1999; In Final Form: August 31, 1999

The various bilayer structures formed from aqueous mixtures of an anionic (SDS) and a cationic surfactant (DTAB) with identical hydrocarbon C_{12} chains at 40 °C have been investigated using small-angle neutron scattering (SANS) as well as static light scattering (SLS). The SANS data were analyzed using a paracrystal lamellar model with respect to the layer distance distribution and the number of layers in a single cluster. Unilamellar or oligolamellar vesicles form in the most diluted samples in the absence of added salt where the number of layers in a single cluster is found to be 1−3. Beyond the compositions where micelles form (30:70 < [SDS]:[DTAB] < 70:30), we observe a transition from vesicles to stacks of lamellar sheets upon increasing the overall surfactant concentration, indicated by an abrupt increase of the number of layers in a single cluster from 1−3 to infinity. Combined SANS and SLS data for samples containing vesicles ([SDS] + [DTAB] = 0.25 wt % in the absence of added salt) could be fitted with a model for unilamellar vesicles using a structure factor for sticky hard spheres, indicating that the vesicles attract each other and form clusters. However, at [SDS] + [DTAB] = 0.125 wt %, the vesicles appeared to be too large for the size distribution to be determined from our SANS and SLS data. In 0.1 M NaBr, the vesicles were clearly destabilized and either micelles or lamellar sheets form at most compositions and concentrations where vesicles predominate in the absence of added salt.

Introduction

As a result of the unfavorable interface between hydrocarbon and water, ionic surfactants aggregate above a certain concentration in an aqueous solvent, forming a dispersed phase. The aggregates have liquidlike cores of hydrocarbon tails, with the charged headgroups located at the hydrocarbon/water interfaces and a diffuse layer of counterions outside. The hydrophobic contribution to the free energy of forming a surfactant aggregate tends, because of geometrical packing constraints, to decrease the curvature of the aggregate interface in order to minimize the hydrocarbon/water contact area per aggregated monomer. There is, however, a large counteracting contribution due to electrostatics as the volume occupied by the diffuse layer of counterions and, consequently, the entropy of mixing counterions and solvent increase with increasing curvature of the aggregate interface. Hence, in a water mixture of a pure ionic surfactant with a moderately sized tail, e.g., sodium dodecyl sulfate (SDS, anionic surfactant) or dodecyltrimethylammonium bromide (DTAB, cationic surfactant), rather small, almost spherical micelles form. However, by means of mixing two oppositely charged surfactants (e.g., SDS and DTAB) in an aqueous solvent, the surface charge densities of the mixed aggregates become dramatically reduced and, as a result, the micelles grow and, at a sufficiently low surface charge density, various bilayer structures spontaneously form, including geometrically closed vesicles.[1−6]

The driving force for the geometrical closure of comparatively large bilayer fragments and the formation of vesicles is the elimination of the unfavorable edges of the bilayer. There is, however, a price for this in terms of a size independent positive work of bending the bilayer.[7] A rather polydisperse collection of thermodynamically stable vesicles is then able to form mainly as a result of a competition between the entropy of mixing aggregates and solvent, tending to decrease the vesicle size, and a constant positive bending work ($=4\pi k_{bi}$), tending to increase the size of the vesicles.[8] Two of the contributions to the bilayer bending constant k_{bi} appear to be more important than the others for a charged vesicle:[9] Geometrical packing constraints give rise to the main positive contribution, tending to increase the aggregate size, whereas a counteracting effect arises from the largest negative contribution which is due to electrostatics. In other words, the unfavorable hydrocarbon/water interfacial tension tends to lower the curvature of the vesicles, whereas the entropy of mixing counterions and solvent tends to increase it.

For vesicles much larger than the bilayer thickness (2ξ), a change in the first order correction to the curvature free energy

* Address for correspondence: Institute for Surface Chemistry, Box 5607, SE-114 86 Stockholm, Sweden. Telephone: +46 8 790 99 41. Fax: +46 8 20 89 98. E-mail: magnus.bergstrom@surfchem.kth.se.

† Present address: Department of Physics and Astronomy, The University of Edinburgh, Mayfield Road, Edinburgh EH9 3JZ, U.K.

10.1021/jp991846w CCC: $18.00
Published on Web 10/27/1999

of the outer monolayer is exactly cancelled by an opposite change for the inner layer and, consequently, terms proportional to the vesicle radius (R) are exactly cancelled as the free energy of a single vesicle ($=4\pi[k_{bi} + 2\gamma_\infty R^2]$, where γ_∞ is the free energy per unit area of an infinitely large planar bilayer) is calculated from a Taylor expansion to second order in curvature.[8,9] However, as the size of the vesicle reaches the order of magnitude of ξ, asymmetries between the outer and inner layers become important. Hence, vesicles stabilized by higher-order bending terms, which give rise to a minimum in the local free energy, must have a size of the order of magnitude of the bilayer thickness, a fact that was not taken into consideration in the frequently quoted theory by Safran et al.[10,11] The importance of mixing for the formation of vesicles was, however, established by these authors.

The exponent α in the vesicle size distribution $\propto R^\alpha \exp[-4\pi(k_{bi} + 2\gamma_\infty R^2)]$ depends on the assumed physical structure of the vesicles. α has been calculated regarding the vesicles shaped as geometrically closed undulating bilayers with a persistence length of the order of magnitude of the size of a surfactant molecule,[12] as well as for a closed bilayer with a sufficiently large persistence length, i.e., of the order of magnitude of the size of a single vesicle, for oblate−prolate shape fluctuations to be the only significant deviation from a strictly spherical geometry.[11]

In a recent paper,[13] we have presented the various microstructures formed in a mixture of SDS and DTAB, i.e., two surfactants with identical hydrocarbon chains, in D_2O at 40 °C using small-angle neutron scattering (SANS) [cf. Figure 1a], and more recently, we have also investigated the same surfactants at the same temperature as they are mixed in a 0.1 M NaBr solution [cf. Figure 1b]. The micelles appeared to be shaped as tablets with a distinct thickness, width, and length, respectively, which in the case of added salt can grow in length to form long flexible ribbonlike particles.[14,15] The micelles were seen to grow in size with decreasing surface charge density as equimolar composition is approached both in pure D_2O and in 0.1 M NaBr, and eventually, a transition to either stacks of lamellar sheets or vesicles occurs.

There is always a certain amount of surfactants existing as free monomers in the surrounding bulk solution, the concentrations of which are determined by equilibrium conditions according to which the chemical potentials in bulk solution and in the aggregates are equal for each surfactant. As the chemical potential in the aggregates of the surfactant in excess, which entirely contributes to the surface charge density, is much larger than the corresponding chemical potential of the surfactant in deficit, the free monomer concentration of the former is several orders of magnitude larger as compared with the latter.[15] Hence, when the samples are diluted at low surfactant concentrations and the fraction of surfactants existing as free monomers increases, the composition in the aggregates changes so that the surface charge densities of anionic-rich as well as cationic rich aggregates decreases. This explains our observation of a slight growth of the micelles upon decreasing the overall surfactant concentration, $c_{surf}^{tot} \equiv$ [SDS] + [DTAB], at a fixed overall composition, $X \equiv$ [SDS]/([SDS] + [DTAB]). Subsequently, a transition from micelles to vesicles occurs in a similar way as when $X \rightarrow 0.5$ for a fixed c_{surf}^{tot}. As the samples are further diluted, an increasing amount of a precipitate (DTA^+DS^-) is formed. A changing composition in surfactant aggregates with increasing concentration for fixed values of the overall surfactant composition, as well as a transition from vesicles to micelles, has recently been observed more directly by Villeneuve et al. from surface tension measurements of mixtures of sodium decyl sulfate and decyltrimethylammonium bromide at 25 °C.[16]

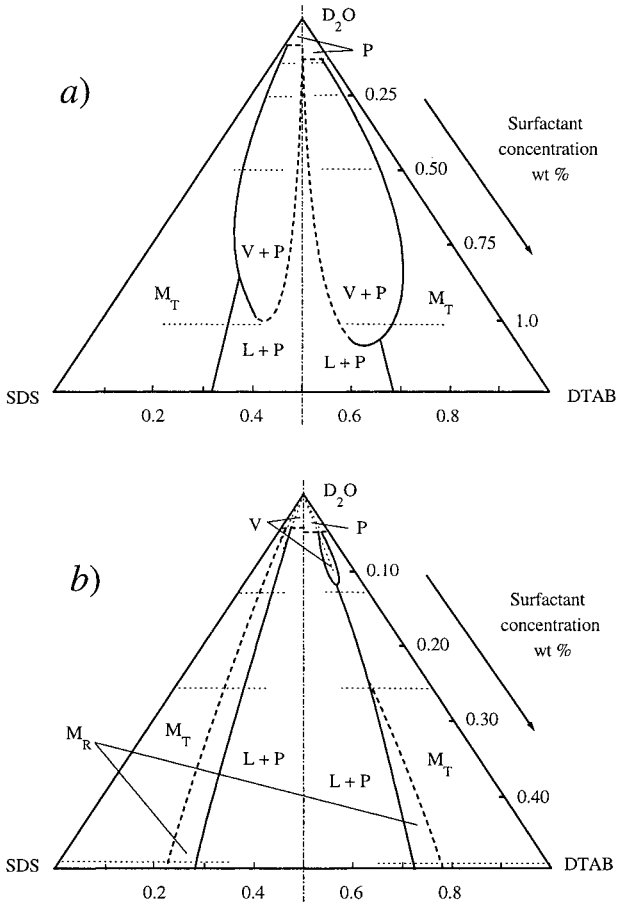

Figure 1. Ternary diagrams showing the regimes of different microstructures found in mixtures of SDS and DTAB using either (a) pure D_2O or (b) 0.1 M NaBr in D_2O as solvent. Several samples along the dotted lines were measured. In the former case, we have found unilamellar or oligolamellar vesicles (V), rigid tablet-shaped micelles (M_T), and stacks of lamellar sheets (L). In the most dilute parts and close to equimolar composition, an increasing amount of a precipitate (P) of DTA^+DS^- is formed. In the case (b) where a monovalent salt was added, some of the micelles were seen to become very elongated and the corresponding scattering data must be fitted with a model for flexible ribbonlike micelles (M_R). There are no sharp boundaries between the regimes where micelles and vesicles are found, but there are rather narrow domains where the two surfactant aggregates coexist. The dashed lines between [SDS]:[DTAB] = 40:60 and 60:40 in the absence of added salt were extrapolated in a similar way as was found by Kaler et al. [cf. ref 2], as we have not measured any samples in this regime. Note the different scales in the two diagrams for the axes denoting the surfactant concentration.

Our SANS results as to the formation of tablet-shaped and ribbonlike micelles have already been presented elsewhere.[14,15] Below we give a detailed account of our findings when investigating samples containing either vesicles or stacks of lamellar sheets using SANS and static light scattering (SLS).

Methods and Materials

Methods. The major part of the SANS experiments were performed on the SANS instrument at the DR3 reactor at Risø National Laboratory, Roskilde, Denmark.[17] A range of scattering vectors (q) from 0.004 to 0.5 $Å^{-1}$ was covered by four combinations of neutron wavelength (3 and 10 Å) and sample-to-detector distances (1-6 m). The wavelength resolution was 18% (full width at half maximum value). Some of the samples

TABLE 1: Results from SANS Data Analyses of Samples Where Mixed SDS/DTAB Bilayer Structures Form at 40 °C in D_2O in the Absence of Added Salt[a]

	[SDS]:[DTAB]											
	20:80	25:75	30:70	32:68	35:65	40:60	60:40	65:35	68:32	70:30	75:25	80:20
5.0% wt %	micelles	not measd	micelles	not measd	micelles, lamellae	two phases	$\xi = 13.5$ $\langle D\rangle = 199$ $P = 0.63$ $N_L = \infty$	$\xi = 13.0$ $\langle D\rangle = 250$ $P = 0.54$ $N_L = \infty$	not	micelles	not	micelles
2.5 wt %	micelles	not measd	micelles	not measd	$\xi = 13.8$ $\langle D\rangle = 214$ $P = 0.42$ $N_L = \infty$	$\xi = 14.3$ $\langle D\rangle = 243$ $P = 0.79$ $N_L = \infty$	$\xi = 13.7$ $\langle D\rangle = 188$ $P = 0.70$ $N_L = \infty$	$\xi = 13.1$ $\langle D\rangle = 226$ $P = 0.89$ $N_L = \infty$	not measd	micelles	not measd	micelles
1.0 wt %	micelles	micelles	micelles, vesicles	micelles, vesicles	$\xi = 14.4$ $\langle D\rangle = 279$ $P = 0.85$ $N_L = 13.8$	$\xi = 14.6$ $\langle D\rangle = 353$ $P = 0.54$ $N_L = 2.54$	$\xi = 14.0$ $\langle D\rangle = 196$ $P = 0.70$ $N_L = \infty$	$\xi = 13.4$ $\langle D\rangle = 305$ $P = 0.77$ $N_L = \infty$	$\xi = 12.4$ $\langle D\rangle = 142$ $P = 0.85$ $N_L = \infty$	micelles, vesicles	micelles	micelles
0.50 wt %	$\xi = 13.3$ $\langle D\rangle = 497$ $P = 0.56$ $N_L = 1.00$	$\xi = 13.8$ $\langle D\rangle = 412$ $P = 0.36$ $N_L = 1.81$	$\xi = 14.7$ $\langle D\rangle = 425$ $P = 0.42$ $N_L = 1.51$	$\xi = 13.5$ $\langle D\rangle = 408$ $P = 0.53$ $N_L = 1.64$	$\xi = 14.8$ $\langle D\rangle = 419$ $P = 0.38$ $N_L = 2.22$	$\xi = 14.8$ $\langle D\rangle = 416$ $P = 0.34$ $N_L = 2.24$	$\xi = 13.8$ $\langle D\rangle = 387$ $P = 0.35$ $N_L = 1.65$	$\xi = 13.7$ $\langle D\rangle = 408$ $P = 0.38$ $N_L = 1.39$	$\xi = 12.8$ $\langle D\rangle = 387$ $P = 0.44$ $N_L = 1.66$	$\xi = 13.2$ $\langle D\rangle = 473$ $P = 0.53$ $N_L = 1.35$	micelles, vesicles	micelles
0.25 wt %	$\xi = 14.0$ $\langle D\rangle = 496$ $P = 0.30$ $N_L = 1.63$	$\xi = 14.1$ $\langle D\rangle = 561$ $P = 0.54$ $N_L = 1.18$	$\xi = 13.7$ $\langle D\rangle = 643$ $P = 0.25$ $N_L = 1.66$	$\xi = 13.2$ $\langle D\rangle = 464$ $P = 0.29$ $N_L = 1.73$	$\xi = 13.8$ $\langle D\rangle = 597$ $P = 0.31$ $N_L = 1.57$	$\xi = 14.1$ $\langle D\rangle = 582$ $P = 0.34$ $N_L = 1.52$	$\xi = 13.6$ $\langle D\rangle = 475$ $P = 0.27$ $N_L = 1.67$	$\xi = 13.4$ $\langle D\rangle = 440$ $P = 0.59$ $N_L = 1.00$	$\xi = 13.2$ $\langle D\rangle = 421$ $P = 0.20$ $N_L = 1.72$	$\xi = 13.4$ $\langle D\rangle = 400$ $P = 0.18$ $N_L = 1.79$	$\xi = 13.4$ $\langle D\rangle = 399$ $P = 0.40$ $N_L = 1.60$	$\xi = 13.2$ $\langle D\rangle = 440$ $P = 0.60$ $N_L = 1.28$
0.125 wt %	$\xi = 13.5$ $\langle D\rangle = 612$ $P = 0.42$ $N_L = 1.40$	$\xi = 14.1$ $\langle D\rangle = 653$ $P = 0.45$ $N_L = 1.33$	$\xi = 14.0$ $\langle D\rangle > 1000$	not measd	$\xi = 13.7$ $\langle D\rangle = 837$ $P = 0.18$ $N_L = 1.71$	$\xi = 13.9$ $\langle D\rangle > 1000$	$\xi = 14.0$ $\langle D\rangle = 597$ $P = 0.13$ $N_L = 1.70$	$\xi = 14.1$ $\langle D\rangle = 594$ $P = 0.13$ $N_L = 1.76$	$\xi = 13.7$ $\langle D\rangle = 597$ $P = 0.13$ $N_L = 1.75$	$\xi = 13.7$ $\langle D\rangle = 565$ $P = 0.11$ $N_L = 1.72$	$\xi = 13.7$ $\langle D\rangle = 464$ $P = 0.25$ $N_L = 1.80$	$\xi = 12.7$ $\langle D\rangle = 479$ $P = 0.17$ $N_L = 1.69$

[a] The data were fitted with a paracrystal lamellar model with an average layer distance $\langle D\rangle$, relative standard deviation of the layer distance distribution $P \equiv \sigma_D/\langle D\rangle$, and a half bilayer thickness ξ. The number of layers in a single aggregate N_L abruptly becomes equal to infinity as a transition from oligolamellar vesicles to stacks of lamellar sheets occur. All spatial dimensions are given in angstroms (Å). The samples were stored 20−25 h at 40 °C before being measured, except the ones at $X = 0.30$, 0.40, 0.60, and 0.70 which were stored 10−15 h.

were also measured on the D22 SANS instrument at Institut Laue-Langevin (ILL), Grenoble, France.[18] The range of scattering vectors between 0.0015 and 0.4 $Å^{-1}$ was covered by three combinations of neutron wavelengths (8 and 12 Å) and sample-to-detector distances (1.4−18 m), and the wavelength resolution was 10%.

The samples investigated with SANS were kept in quartz cells (Hellma) with a path length of either 2, 5, or 10 mm depending on the surfactant concentration. The raw spectra were corrected for background from the solvent, sample cell, and other sources by conventional procedures.[19] The two-dimensional isotropic scattering spectra were azimuthally averaged, converted to an absolute scale, and corrected for detector efficiency by dividing by the incoherent scattering spectra of pure water.[20] The scattering intensity was furthermore normalized by dividing with the concentrations of solute (SDS and DTAB) in the surfactant aggregates.

The average excess scattering length density per unit mass ($\Delta\rho_m$) of the solute was calculated from the known SDS-to-DTAB molar ratios using the appropriate molecular volumes and molecular weights of the monomers.[21]

Throughout the SANS data analysis, corrections were made for instrumental smearing.[17,22] For each instrumental setting, the ideal model scattering curves were smeared by the appropriate resolution function when the model scattering intensity was compared with the measured one by means of least-squares methods. The parameters in the model were optimized by means of conventional least-squares analyses and the errors of the parameters were calculated by conventional methods.[23,24] Some of the samples were measured more than once in order to check the reproducibility of our results.

Static light scattering (SLS) measurements were performed at ETH, Zürich, Switzerland, with a commercial goniometer system (ALV/DLS/SLS-5000F monomode fiber compact goniometer system with ALV-5000 fast correlator). The instrument had been modified to allow for a much larger temperature range (−6 to 200 °C) and increased temperature stability (better than ±0.01 °C for several hours). Approximately 1 mL of the solution was transferred into the cylindrical scattering cell (10 mm diameter). The scattering cell was then stoppered and centrifuged for approximately 30 min at 5000g and 40 °C in order to remove dust particles from the scattering volume. Experiments were performed at 69 different angles between $15° \le \theta \le 151°$, corresponding to q values in the range 4.48×10^{-4} $Å^{-1} \le q \le 33.2 \times 10^{-4}$ $Å^{-1}$, and 3 individual measurements were taken and averaged for each angle. The data were then corrected into absolute scale intensities using toluene as a reference standard.[25,26] In the data analyses, a few of the highest and lowest data points were omitted so that the regime of SLS data analyzed was approximately 5.5×10^{-4} $Å^{-1} \le q \le 30 \times 10^{-4}$ $Å^{-1}$.

Materials. Sodium dodecyl sulfate (SDS) (99% purity) was obtained from Merck and 99% dodecyltrimethylammonium bromide (DTAB) from Aldrich Chemical Company. In the SANS measurements, we used 99% sodium bromide (NaBr) and D_2O with 99.9 atom % D from Aldrich. In the SLS measurements, we used 99% sodium bromide from Fluka AG and 99.75% D_2O from Merck as well as 99.8% D_2O from Dr. Glaser AG Basel. All chemicals were used without further purification.

Sample Preparation. Stock solutions containing SDS and DTAB in pure D_2O ranging from $X = 0.15$ to $X = 0.40$ and from $X = 0.60$ to $X = 0.85$ were prepared by simply mixing D_2O solutions of SDS and DTAB in the right proportions so as to yield an overall surfactant concentration (c_{surf}^{tot}) of about 1.0 or 5.0 wt %. D_2O was chosen in order to minimize the

TABLE 2: Results from SANS Data Analyses of Samples Where Mixed SDS/DTAB Bilayer Sheets Form at 40 °C in 0.1 M NaBr[a]

	[SDS]:[DTAB]					
	25:75	30:70	35:65	65:35	70:30	75:25
1.0 wt %	micelles	micelles	$\xi = 13.2$ $\langle D\rangle = 216$ $P = 0.93$	$\xi = 12.7$ $\langle D\rangle = 230$ $P = 0.98$	$\xi = 12.3$ $\langle D\rangle = 83$ $P = 0.86$	micelles
0.50 wt %	micelles	$\xi = 13.1$ $\langle D\rangle = 91$ $P = 0.88$	$\xi = 13.3$ $\langle D\rangle = 225$ $P = 0.96$	$\xi = 12.5$ $\langle D\rangle = 226$ $P = 0.99$	$\xi = 12.1$ $\langle D\rangle = 91$ $P = 0.92$	micelles
0.25 wt %	$\xi = 12.7$ $\langle D\rangle = 105$ $P = 0.88$	$\xi = 13.4$ $\langle D\rangle = 235$ $P = 1.02$	$\xi = 13.9$ $\langle D\rangle = 173$ $P = 0.85$	$\xi = 12.8$ $\langle D\rangle = 207$ $P = 1.01$	vesicles	micelles
0.125 wt %	$\xi = 13.3$ $\langle D\rangle = 152$ $P = 0.85$	$\xi = 13.1$ $\langle D\rangle = 179$ $P = 0.78$	not measured	not measured	vesicles	$\xi = 12.1$ $\langle D\rangle = 82$ $P = 0.90$

[a] The data were fitted with a paracrystal lamellar model with an average layer distance $\langle D\rangle$, relative standard deviation of the layer distance distribution $P \equiv \sigma_D/\langle D\rangle$, and half bilayer thickness ξ. The number of layers in a single aggregate N_L was equal to infinity for all the analyzed samples. Somewhat higher χ^2 values for the fits of the samples closest to the domains where micelles are observed indicate that small amounts of (ribbonlike) micelles may coexist with the lamellar sheets. All spatial dimensions are given in angstroms (Å). The samples were stored 20−25 h at 40 °C before being measured.

incoherent background from hydrogen and obtain a high scattering contrast in the SANS experiments. The brine was prepared by mixing NaBr in D_2O with a concentration of 0.1 M. Then SDS and DTAB with proportions ranging from $X = 0.1$ to $X = 0.35$ and from $X = 0.65$ to $X = 0.9$ were mixed in the brine to give $c_{surf}^{tot} = 1.0$ wt %. The final samples were then obtained by means of diluting the stock solutions to various surfactant concentrations (c_{surf}^{tot}= 5.0, 2.5 (no added salt), 1.0, 0.50, 0.25, and 0.125 wt %) and slightly shaken in order to evenly distribute the various components in the solutions. We have also measured $X = 0.15$, 0.20, 0.80, and 0.85 at $c_{surf}^{tot} = 0.05$ and 0.025 wt % (brine) at ILL and $X = 0.85$ at $c_{surf}^{tot} = 0.05$, 0.04, 0.03, and 0.025 wt % (brine) at Risø. After it had been established at which compositions and concentrations vesicles form, the samples measured more than once were prepared by making stock solutions with a surfactant concentration equaling the highest where vesicles were found. At ETH we measured the following samples with SLS: $X = 0.15$, 0.20, 0.25, 0.30, 0.70, 0.75, 0.80, and 0.85 at $c_{surf}^{tot} = 0.125$ and 0.25 wt % in the absence of added salt and the same compositions (i.e. X) at $c_{surf}^{tot} = 0.025$ and 0.05 wt % in 0.1 M NaBr. The samples measured at Risø were stored 20−25 h at 40 °C with the purpose of equilibration before the experiments, except the samples for which $X = 0.30$, 0.40, 0.60, and 0.70 in the absence of added salt which were stored 10−15 h before the measurements. In addition, the samples in which vesicles were found at $X = 0.20$ and 0.80 were measured at Risø after 10−15 h and three of the samples ([$X = 0.20$, $c_{surf}^{tot} = 0.50$ wt %], [$X = 0.75$, $c_{surf}^{tot} = 0.25$ wt %], and [$X = 0.80$, $c_{surf}^{tot} = 0.25$ wt %]) after seven days. From the SLS data, it appeared that the vesicles form clusters of aggregates (see further below). In an attempt to prevent this cluster formation, the samples measured at ILL ([$X = 0.20$, $c_{surf}^{tot} = 0.125$, 0.25, and 0.50 wt %], [$X = 0.75$, $c_{surf}^{tot} = 0.25$ wt %], [$X = 0.80$, $c_{surf}^{tot} = 0.125$ and 0.25 wt %], [$X = 0.85$, $c_{surf}^{tot} = 0.125$ wt %] in addition to the ones mentioned above) were only stored for 5−10 h at 40 °C before being measured. Nevertheless, the vesicles were seen to have started forming clusters already after a few hours. The samples measured with SLS were all stored 20−25 h at 40 °C, and the sample [$X = 0.75$, $c_{surf}^{tot} = 0.25$ wt %] was also measured after 7 days. The temperature was chosen to be sufficiently high for a precipitate of DTA^+SDS^- to be dissolved in the investigated SDS-to-DTAB molar ratios, although small amounts of precipitate were found in the most diluted samples [cf. further above]. Bilayer structures were found at the surfactant compositions and concentrations indicated in Tables 1 and 2 and in the ternary diagrams in Figure 1.

The mixed catanionic surfactant aggregates we have studied form spontaneously upon simply mixing the various species, without need to supply energy in any form, and the various structures are believed to be thermodynamically stable.[2] This is supported by our observation that a significant structural change of the aggregates occurs within comparatively short times upon simply diluting the samples.

Results and Discussion

Analyses of the SANS Data Using a Paracrystal Lamellar Model. All samples containing any multibilayer structure could, within the q range measured at Risø, be fitted with a paracrystal lamellar model[27,28] for which the scattering cross section can be written as follows:

$$\frac{d\sigma(q)}{d\Omega} = 2\pi\Delta\rho_m{}^2\Gamma_m\frac{P_{bil}(q)}{q^2}Z_N(q) \qquad (1)$$

where $\Delta\rho_m$ is the difference in scattering length per unit mass of solute between particles and solvent and Γ_m is the mass per area of the bilayer. The form factor is here separated into one contribution that accounts for the cross section of a planar bilayer

$$P_{bil}(q) = \left(\frac{\sin(q\xi)}{q\xi}\right)^2 \qquad (2)$$

where ξ is half the bilayer thickness, and a factor proportional to q^{-2} which is typical for an infinitely large two-dimensional sheet. The latter can be employed as the aggregates are much larger than what can be determined from our SANS data. $Z_N(q)$ describes the interference effects for aggregates consisting of more than one layer, and it can be written as a function of the average number of layers, $N_L = x_N N + (1 - x_N)(N + 1)$, of two clusters consisting of N integer number of layers the fraction of which is x_N and $N + 1$ layers, the fraction of which is $1 - x_N$, respectively. This means that, for example, $N_L = 2.3$ denotes a mixture of 70% $N = 2$ and 30% $N = 3$. Such aggregates might consist of either oligolamellar large vesicles or clusters

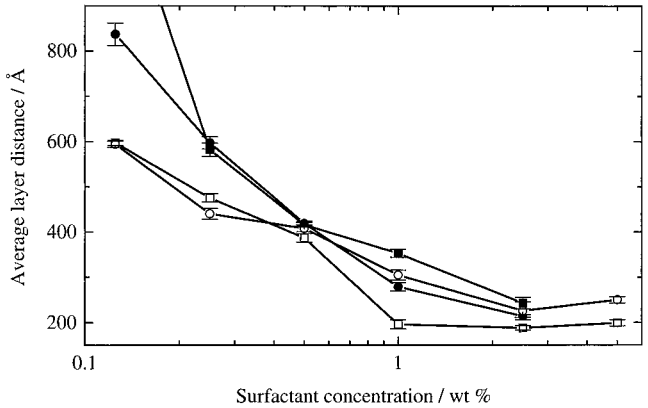

Figure 2. Average layer distance $\langle D\rangle$, with error bars, as obtained from a fit with a paracrystal lamellar model plotted against the overall surfactant concentration for DTAB-rich samples (solid symbols) and SDS-rich samples (open symbols) at surfactant compositions X and $1 - X = 0.35$ (circles) and X and $1 - X = 0.40$ (squares). The average layer distance at $X = 0.40$ and $c_{\text{surf}}^{\text{tot}} = 0.125$ wt % was too large to be determined from our SANS data.

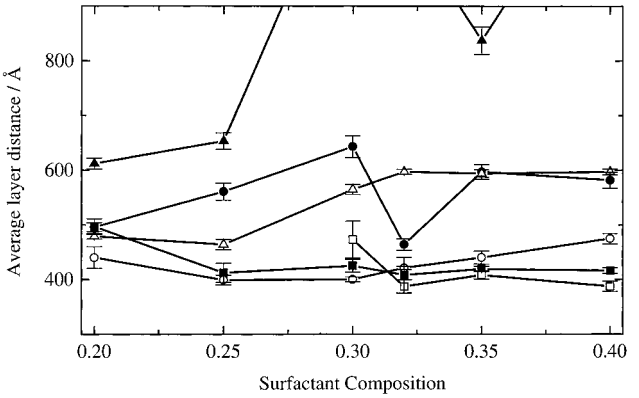

Figure 3. Average layer distance $\langle D\rangle$, with error bars, as obtained from a fit with a paracrystal lamellar model plotted against the surfactant composition X for DTAB-rich samples (solid symbols) and $1 - X$ for SDS-rich samples (open symbols) at overall surfactant concentrations 0.125 wt % (triangles), 0.25 wt % (circles), and 0.50 wt % (squares). The average layer distances at $X = 0.30$ and 0.40 at $c_{\text{surf}}^{\text{tot}} = 0.125$ wt % were too large to be determined from our SANS data.

of unilamellar vesicles or, possibly, a combination of the two (see further below). Hence, we write[27,28]

$$Z_N(q) = \frac{1 - w^2}{1 + w^2 - 2w\cos(q\langle D\rangle)} + x_N S_N + (1 - x_N)S_{N+1} \tag{3}$$

where

$$S_N(q) = a_N/N[1 + w^2 - 2w\cos(q\langle D\rangle)]^2 \tag{4}$$

and

$$a_N = 4w^2 - 2(w^3 + w)\cos(q\langle D\rangle) - 4w^{N+2}\cos(Nq\langle D\rangle) + 2w^{N+3}\cos[(N-1)q\langle D\rangle] + 2w^{N+1}\cos[(N+1)q\langle D\rangle] \tag{5}$$

where the average distance between two adjacent layers, $\langle D\rangle$, and a relative standard deviation, $P \equiv \sigma_D/\langle D\rangle$, of the Gaussian layer distance distribution, $w = \exp[-\sigma_D{}^2q^2/2]$, are included in the factor.

An overview of the results from our analyses using the paracrystal lamellar model is given in Table 1 for the case where no extra salt was added. Apart from the parameters given in Table 1, the data were fitted with respect to the mass per area (Γ_m) and the residual background. The number of layers appeared to be rather small for $c_{\text{surf}}^{\text{tot}}$ lower than about 0.25−0.5 wt %; i.e., N_{L} was found to be between 1.0 and 2.5, indicating that one or two small unilamellar vesicles are enclosed by one larger. There are tendencies of increasing $\langle D\rangle$ when the samples are diluted at a given X [cf. Figure 2] or, to a less extent, when the equimolar composition is approached at a given $c_{\text{surf}}^{\text{tot}}$ [cf. Figure 3], most probably caused by an increase of the sizes of the vesicles. In addition, samples containing vesicles at $X =$ 0.20 and 0.80 were also measured after 10−15 h (not given in the table). Three of the samples containing vesicles ([$X = 0.20$, $c_{\text{surf}}^{\text{tot}} = 0.50$ wt %], [$X = 0.75$, $c_{\text{surf}}^{\text{tot}} = 0.25$ wt %] and [$X =$ 0.80, $c_{\text{surf}}^{\text{tot}} = 0.25$ wt %]) were also measured after about 1 week. In all of these samples, the number of layers appeared to increase slightly with time from $N_{\text{L}} = 1.0$ at about 10−15 h to $N_{\text{L}} = 1.3$ after 1 week [$X = 0.20$, $c_{\text{surf}}^{\text{tot}} = 0.50$ wt %], from N_{L} $= 1.6$ (20−25 h) to 1.9 [$X = 0.75$, $c_{\text{surf}}^{\text{tot}} = 0.25$ wt %] and from $N_{\text{L}} = 1.0$ (10−15 h) to 1.4 [$X = 0.80$, $c_{\text{surf}}^{\text{tot}} = 0.25$ wt %]. The variations of $\langle D\rangle$, $\sigma_{\text{D}}/\langle D\rangle$, and ξ with the time the samples were stored before being measured, were seen to be small and unsystematic. A rapid dilution of a sample containing micelles [$X = 0.20$, $c_{\text{surf}}^{\text{tot}} = 5.0$ wt %] to a concentration where vesicles spontaneously form [$X = 0.20$, $c_{\text{surf}}^{\text{tot}} = 0.50$ wt %] followed by regular measurements with SANS shows that vesicles predominate within the time it takes to start the measurement (1−3 min) and that the appearance of the scattering data with q larger than about 0.01, which can be measured within a reasonably short time span, does not change within a week.

When the mass per area (Γ_{m}) obtained from our model fits is compared with the same quantity as calculated from the thickness of the bilayers, it is evident that the amount of particles observed in our measurements is substantially less than the amount of surfactants added to the sample. The observed volume fraction of SDS-rich particles is larger than the corresponding quantity of DTAB-rich particles, and in both cases, it increases when extra salt is added to the solutions. Moreover, the concentration of aggregates increases as the equimolar composition is approached at a fixed $c_{\text{surf}}^{\text{tot}}$, and the amount of observed particles relative to the amount of added surfactant decreases with decreasing $c_{\text{surf}}^{\text{tot}}$ at a fixed X. All these observations are mainly due to the fact that certain amounts of the surfactants appear as free monomers as described in the introduction of this paper. The formation of small amounts of a precipitate (DTA^+DS^-) observed in the DTAB-rich samples in the absence of added salt certainly also contributes somewhat to the material loss. However, other kinds of aggregates such as micelles coexisting with the lamellar structures could only be observed in a few of the samples as indicated in Table 1. The material loss was estimated from the absolute scattering intensities to about 40% for DTAB-rich samples and 25% for SDS-rich samples in the absence of added salt. The fraction of surfactant that does not contribute to the scattering intensity increases slightly with decreasing surfactant concentration.

When the overall surfactant concentration is raised above about 1 wt % (DTAB-rich samples) or 0.5 wt % (SDS-rich samples) in the absence of added salt for samples where $0.30 < X < 0.70$, N_{L} is found to reach infinity, and hence, we could fit the data with

$$Z(q) = \frac{1 - w^2}{1 + w^2 - 2w\cos(q\langle D\rangle)} \tag{6}$$

instead of $Z_N(q)$ in eq 1 [cf. Table 1]. We have interpreted the

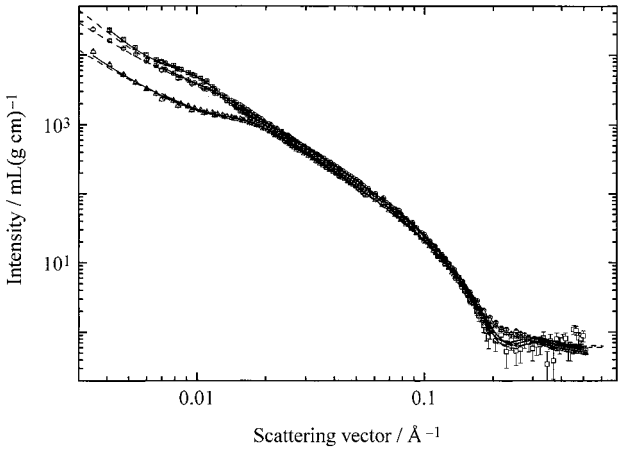

Figure 4. Normalized scattering intensity as a function of the scattering vector q for samples with an overall surfactant concentration 0.125 wt % (upper lines, squared symbols), 1.0 wt % (middle lines, circular symbols), and 5.0 wt % (lower lines, triangular symbols), respectively, at a given surfactant molar ratio [SDS]:[DTAB] = 65:35. Individual symbols represent SANS data obtained with different combinations of neutron wavelength and sample−detector distance at Risø. The lines represent the results from fits with a paracrystal lamellar model which describes the formation of oligolamellar vesicles, at 0.125 wt %, with an average distance between two adjacent bilayers $\langle D\rangle = 594$ Å, a relative standard deviation of the layer distance distribution $\sigma_D/\langle D\rangle = 0.13$, half bilayer thickness $\xi = 14.1$ Å, and a total number of layers in a single aggregate $N_L = 1.76$. The agreement of the fit[23] as measured by χ^2 is 4.2. For the surfactant concentrations 1.0 and 5.0 wt %, the number of layers equals infinity and $\langle D\rangle = 305$ Å, $\sigma_D/\langle D\rangle = 0.77$, $\xi = 13.4$ Å, $\chi^2 = 8.8$ (1.0 wt %) and $\langle D\rangle = 250$ Å, $\sigma_D/\langle D\rangle = 0.54$, $\xi = 13.0$ Å, $\chi^2 = 85$ (5.0 wt %). The large value of χ^2 at 5.0 wt % is mainly due to the very good statistics of the SANS data at such high surfactant concentrations in the regime of very high q values containing information about distances of the order of magnitude of molecular size. The solid lines correspond to the intensity smeared by the instrumental resolution, and the dashed lines correspond to the ideal intensity.

result as the occurrence of a transition between vesicles and stacks of (disordered) lamellar sheets caused by significant interactions between the vesicles that become overpacked above a certain overall surfactant concentration. The difference in surfactant concentration where the transition from vesicles to lamellar sheets occur between SDS-rich and DTAB-rich aggregates is consistent with the fact that the free monomer concentration of DTAB is about twice the corresponding quantity for SDS (the critical micelle concentration equals 16 mM for pure DTAB and 8 mM for pure SDS at 25 °C). Examples of scattering data for samples with different overall surfactant concentrations at $X = 0.65$, containing either vesicles or lamellae, are given in Figure 4 together with fits using the paracrystal lamellar model. The different appearance of the scattering behavior in the q regime below about 0.01 between large oligolamellar vesicles (squares) and lamellar sheets (circles and triangles) is clearly seen.

In the case where 0.1 M NaBr was used as solvent, a lamellar phase was found in most of the investigated samples not containing micelles [cf. Table 2]. Unilamellar vesicles were, however, observed in DTAB-rich samples ($X = 0.15$ and 0.20) below about $c_{surf}^{tot} = 0.125$ wt % and in SDS-rich samples ($X = 0.80$ and 0.85) below about $c_{surf}^{tot} = 0.05$ wt % [cf. Figure 1b]. From the SANS data, we are able to see that micelles coexist with comparatively large amounts of a precipitate (DTA^+DS^-) at $X = 0.15$ and 0.20 for $c_{surf}^{tot} = 0.05$ wt % and the amount of precipitate increases as the samples are further diluted to $c_{surf}^{tot} = 0.025$ wt %. The formation of micelles rather than any bilayer structures in these samples indicates a change in composition in the aggregates so that the surface charge density increases, favoring micelles over vesicles. The formation of a precipitate in the DTAB-rich samples in brine below about 0.05 wt % surfactant as well as in SDS-rich samples in brine below about 0.025 wt % was readily observed with the bare eye.

The reason for the destabilization of vesicles, and the formation of a lamellar phase, in brine is most probably due to the considerable increase of the work of bending a planar bilayer into a geometrically closed vesicle as the negative contribution from electrostatics vanishes with increasing electrolyte concentration.[8] The average distances between two adjacent layers, $\langle D\rangle$, substantially decrease upon addition of salt, which is probably caused by the decreasing concentration of free monomers as the electrostatic contribution to the chemical potential of the surfactant in excess is reduced. For example, the amount of material loss calculated from the absolute scattering intensities for DTAB-rich samples at $X = 0.35$ and $c_{surf}^{tot} = 1.0$ wt % decreased from 36%, corresponding to 13.9 mM, to 20% (7.6 mM) when 0.1 M NaBr was used as solvent instead of pure D_2O. For SDS-rich samples at $X = 0.65$ and 1.0 wt % surfactant, the corresponding material loss decreased from 23% (9.7 mM) to 2% (0.9 mM). The increasing influence of attractive DLVO interlamellar interactions may also contribute to the observed decrease of $\langle D\rangle$ as electrolyte is added to the solutions. We did not observe any clear variation of $\langle D\rangle$ with c_{surf}^{tot} for samples with $N_L = \infty$ either in pure D_2O or in 0.1 M NaBr, indicating that the samples are inhomogeneous, containing various domains of different microstructures. No evident phase separation could, however, be observed except at [$X = 0.50$, $c_{surf}^{tot} = 5.0$ wt %, no added salt]. In studies of similar systems to the one we have investigated, it was found that lamellar sheets in general was observed to coexist with oligolamellar or multilamellar vesicles. We are inclined to believe that the same holds true for our system, as vesicles rather than lamellar sheets was observed for two samples at $X = 0.70$ in 0.1 M NaBr [cf. Table 2]. The variance of the layer distance distribution was generally seen to be larger in brine, where $\sigma_D/\langle D\rangle \approx 1$, than in the absence of added salt [cf. Tables 1 and 2], indicating an almost exponential layer distance distribution for the weakly interacting bilayers in 0.1 M NaBr.

We find that the thicknesses of all observed lamellar structures are considerably smaller than twice a fully extended hydrocarbon C_{12} chain, consistent with a substantial increase of the conformational entropy for nonstretched chains.[29] Previous detailed model calculations on vesicles formed from a mixture of an anionic and a cationic C_{12} surfactant give half a thickness of the hydrocarbon part of the bilayer of about $\xi = 11$ Å.[30] In analogy to what we found for the tablet-shaped micelles,[14,15] the DTAB-rich bilayers were seen to be somewhat thicker than the SDS-rich bilayers. The main reason for this is the similarity in scattering contrast between the sulfate headgroup and the D_2O and the resemblance of the TA^+ headgroup to the hydrocarbon part of the bilayer. However, the diffuse layer of counterions also contributes somewhat to the bilayer thicknesses given in Tables 1 and 2, which is indicated by the observed decrease of ξ as extra salt was added to the solutions. There is a general trend of a decreasing bilayer thickness with increasing surfactant concentration for the aggregates formed in the absence of added salt [cf. Table 1]. This is in accordance with an increasing area per headgroup as a response to an increasing surface charge density in the bilayers[30] caused by the free monomer effect described above in the Introduction.

Analyses of Combined SANS and SLS Data Using a

TABLE 3: Results from Combined SANS and SLS Data Analyses of Mixed SDS/DTAB Vesicles Formed at 40 °C in D_2O in the Absence of Added Salt[a]

$X = 0.15$	$X = 0.20$	$X = 0.25$	$X = 0.30$	$X = 0.70$	$X = 0.75$	$X = 0.75$*
$\langle R\rangle = 352$	$\langle R\rangle = 418$	$\langle R\rangle = 457$	$\langle R\rangle = 560$	$\langle R\rangle = 429$	$\langle R\rangle = 365$	$\langle R\rangle = 373$
$P = 0.36$	$P = 0.29$	$P = 0.35$	$P = 0.25$	$P = 0.44$	$P = 0.31$	$P = 0.33$
$\xi = 13.9$	$\xi = 14.2$	$\xi = 14.0$	$\xi = 13.7$	$\xi = 13.3$	$\xi = 13.5$	$\xi = 13.9$
$\tau = 0.044$	$\tau = 0.032$	$\tau = 0.063$	$\tau = 0.054$	$\tau = 0.038$	$\tau = 0.030$	$\tau = 0.031$
$\delta/R_{HS} = 0.34$	$\delta/R_{HS} = 0.30$	$\delta/R_{HS} = 0.35$	$\delta/R_{HS} = 0.22$	$\delta/R_{HS} = 0.13$	$\delta/R_{HS} = 0.20$	$\delta/R_{HS} = 0.24$

[a] The overall surfactant concentration [SDS] + [DTAB] equals 0.25 wt % for all the samples. The data were fitted with a model for unilamellar vesicles with a (number weighted) average radius $\langle R\rangle$, relative standard deviation $P \equiv \sigma_R/\langle R\rangle$, and half bilayer thickness ξ. The vesicles appear to attract each other in order to form clusters, and a structure factor for sticky hard spheres with an attractive square well pair potential of depth u and width δ was used. The interaction parameter τ is defined as $\tau^{-1} = 4[\exp(-u/kT) - 1][(1 + \delta/R_{HS})^3 - 1]$, and the hard sphere radius R_{HS} was taken to be 20 Å larger than $\langle R\rangle$. All samples were stored 20−25 hours at 40 °C before the experiments, except the one indicated by an asterisk which was measured after 7 days.

Structure Factor for Sticky Hard Spheres. In order to determine the vesicle size distributions, we have performed static light scattering (SLS) measurements from which the scattering behavior in the regime 5.5×10^{-4} Å$^{-1} < q < 30 \times 10^{-4}$ Å^{-1} is obtained. By means of combining SANS and SLS data in our analyses, we were able to get information from a much wider q range than is possible when only using SANS. From the SLS measurements, it was evident that we could not fit the data with a model for a collection of *noninteracting* vesicles. However, by assuming that the vesicles attract each other in order to form higher-order clusters, we were able to obtain very good agreement between the model and data. Hence, we have used the following expression for the scattering cross section

$$\frac{d\sigma(q)}{d\Omega} = \Delta\rho_m{}^2\langle A\rangle_w\Gamma_m P_{bil}(q)\langle V^2 P_{shell}(q)\rangle[1 + \beta(q)(S(q) - 1)] \quad (7)$$

where it has been assumed that the radius (R) of a vesicle is much larger than half the bilayer thickness (ξ) so that the form factor separates into a thickness and a shell part, P_{bil} and $\langle V^2 P_{shell}(q)\rangle$, respectively. P_{bil} is given by eq 2 and

$$\langle V^2 P_{shell}(q)\rangle = \int N(R)V(R)^2 F(q,R)^2\, dR \quad (8)$$

where V is the volume and $\langle A\rangle_w$ the weight-averaged area of the vesicles and

$$F(q,R) = \sin(qR)/qR \quad (9)$$

is the form factor of an infinitely thin spherical shell. The number weighted vesicle size distribution, $N(R)$, is described by a Schultz distribution with respect to R^2 (i.e., proportional to the aggregation number)

$$N(R) = \frac{2R^{2z+1}}{z!}\left(\frac{z+1}{\langle R^2\rangle}\right)^{z+1} e^{-R^2(z+1)/\langle R^2\rangle} \quad (10)$$

the relative standard deviation of which with respect to R is

$$\frac{\sigma_R}{\langle R\rangle} = \sqrt{\frac{2(\alpha+1)}{\alpha^2}\left[\frac{\Gamma((\alpha+1)/2)}{\Gamma(\alpha/2)}\right]^2 - 1} \quad (11)$$

where $\alpha = 2z + 1$ and $\Gamma(x)$ is the gamma function. $\beta(q)$ is defined as

$$\beta(q) = [\int N(R)V(R)F(q,R)\, dR]^2/\int N(R)V(R)^2 F(q,R)^2\, dR \quad (12)$$

as we in eq 7 have used the decoupling approximation[31] when incorporating a structure factor $S(q)$ for sticky hard spheres[32,33] of radius R_{HS} outside which an attractive square well pair potential of depth u and width δ is located. The structure factor could then be fitted with respect to R_{HS}, δ, and the interaction parameter τ, which is defined by $\tau^{-1} = 4[\exp(-u/kT) - 1][(1 + \delta/R_{HS})^3 - 1]$. In order to simplify the fitting procedure, we have used the approximate and explicit expression for τ as a function of the particle volume fraction and δ/R_{HS} that was given in ref 33.

It is difficult to physically interpret the parameters τ and δ, associated with the structure factor, since in reality the interactions between the vesicles cannot strictly be described with a simple square well potential. According to the DLVO theory, they are rather the result of a balance between long-ranged repulsive double-layer forces and short ranged attractive van der Waals interactions which, at certain electrolyte concentrations, are able to generate a minimum in the interaction potential at a certain distance between two charged colloidal particles.[34]

The results of our analyses of vesicles in the absence of added salt are given in Table 3. The hard sphere radius (R_{HS}) was generally taken to be 20 Å larger than the average bilayer midplane radius, $\langle R\rangle$, and the volume fraction of vesicles was calculated from R_{HS} and the total amount of added surfactant, assuming that the whole amount of surfactant forms vesicles. The last assumption is certainly not correct since an appreciable amount of the surfactants exist as free monomers. However, as we cannot physically interpret the various parameters associated with the intervesicular interactions, we have not found it necessary to estimate the volume fraction of vesicles more accurately. We find from our analyses that the sizes of the DTAB-rich as well as the SDS-rich vesicles increase at $c_{surf}^{tot} = 0.25$ wt % as the equimolar composition is approached, in accordance with an increasing work of bending a planar bilayer into a geometrically closed vesicle with decreasing fraction of the surfactant in excess,[30] i.e., decreasing surface charge density in the bilayer. The relative standard deviation, based on the number-weighted size distribution, $\sigma_R/\langle R\rangle$, varied between 0.24 and 0.44. No clear variation of the polydispersity with surfactant composition could, however, be observed. $\sigma_R/\langle R\rangle$ has been theoretically estimated to be 0.36, corresponding to 0.28 for the volume weighted size distribution, for a collection of noninteracting oblate or prolate shape fluctuating bilayer vesicles.[11] At $c_{surf}^{tot} = 0.125$ wt %, huge bilayer structures, probably vesicles, appeared to have formed with a size that could not be determined from the combined SANS and SLS data.

A sample with an identical composition to one of those measured after 20−25 h was also measured after 7 days with both SANS and SLS, and the results with respect to $\langle R\rangle$ as well as $\sigma_R/\langle R\rangle$ were seen to deviate only slightly between the two samples [cf. Table 3]. The appearance of the SLS data was slightly different after 1 day as compared with after 1 week, indicating that the process of forming higher order clusters of

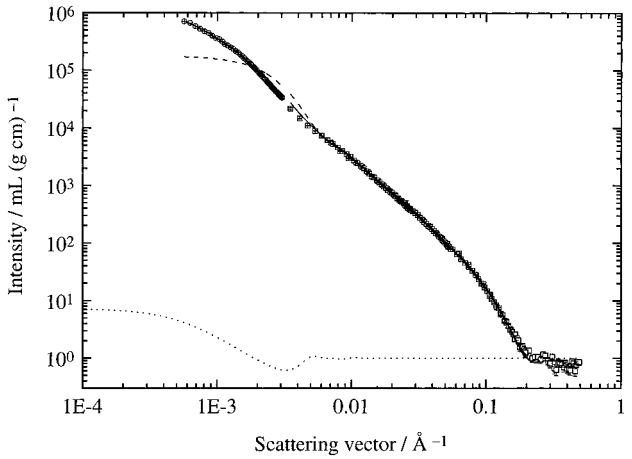

Figure 5. Normalized scattering intensity as a function of the scattering vector q for a sample with surfactant molar ratio [SDS]:[DTAB] = 25:75 at an overall surfactant concentration of 0.25 wt % in the absence of added salt. The squared individual symbols represent SANS data obtained with different combinations of neutron wavelength and sample detector distance at Risø, and the circular symbols represent SLS data. The solid lines represent the results from a fit with a model for polydisperse unilamellar vesicles with a structure factor for sticky hard spheres. The (number-weighted) average radius $\langle R\rangle$ is 457 Å, the relative standard deviation $\sigma_R/\langle R\rangle = 0.35$, and half the bilayer thickness $\xi =$ 14.0 Å. The parameter τ related to the depth of the square potential well equals 0.063, and $\delta/R_{HS} = 0.35$ where δ is the width of the potential well and the hard sphere radius R_{HS} was set equal to $\langle R\rangle +$ 20 Å. The agreement of the fit as measured by χ^2 is 4.9. The dashed line is the contribution to the scattering intensity when $S(q)$ is set equal to unity, and the dotted line is the effective structure factor $S_{eff}(q) \equiv 1 + \beta(q)(S(q) - 1)$.

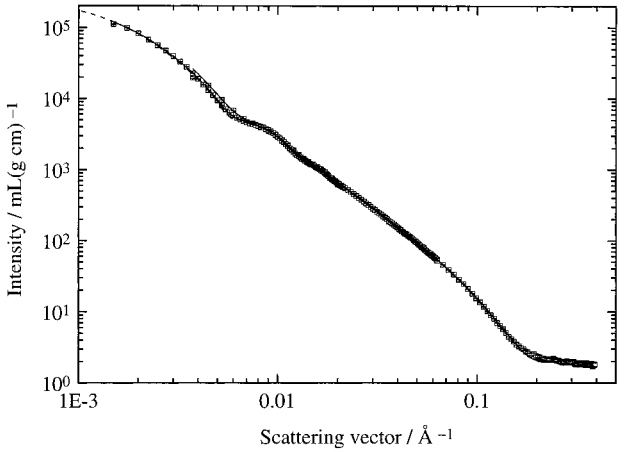

Figure 6. Normalized scattering intensity as a function of the scattering vector q for a sample with surfactant molar ratio [SDS]:[DTAB] = 20:80 at an overall surfactant concentration of 0.50 wt % in the absence of added salt. Individual symbols represent SANS data obtained with different combinations of neutron wavelength and sample detector distance at the ILL. The lines represent the results from a fit with a model for unilamellar vesicles in which a structure factor for sticky hard spheres was used. The (number-weighted) average radius $\langle R\rangle$ is 488 Å, the relative standard deviation $\sigma_R/\langle R\rangle = 0.27$, and half the bilayer thickness $\xi = 14.0$ Å. The parameter τ related to the depth of the square potential well equals 0.020, and $\delta/R_{HS} = 0.36$ where δ is the width of the potential well and the hard sphere radius R_{HS} was set equal to about 20 Å larger than $\langle R\rangle$. The agreement of the fit as measured by χ^2 is 7.7. The solid lines correspond to the intensity smeared by the instrumental resolution, and the dashed lines correspond to the ideal intensity.

vesicles in general takes a longer time than the formation of the vesicles themselves. This may be due to the high free-energy barrier, caused by the repulsive double layer interactions, between two charged aggregates approaching each other. An example of combined SANS and SLS data together with model fits for a sample containing vesicles is given in Figure 5.

It was difficult to fit the low q regime with the sticky hard sphere model for many of the samples measured at ILL, indicating that these samples were not fully equilibrated with respect to cluster formation. Good agreements between data and model fit were nevertheless found for the sample [$X = 0.20$, $c^{tot}_{surf} = 0.50$ wt %] in the absence of added salt [cf. Figure 6] and in 0.1 M NaBr at [$X = 0.20$, $c^{tot}_{surf} = 0.125$ wt %] for which $\langle R\rangle = 423$ Å, $\sigma_R/\langle R\rangle = 0.37$, $\xi = 14.1$ Å, $\tau = 0.032$, and $\delta/R_{HS} = 0.40$.

Coexistence of Micelles and Vesicles. Between the regimes where micelles and vesicles form [cf. Figure 1], there are rather narrow domains where the two kinds of aggregates appear to coexist. The corresponding data can be fitted using the following expression for the scattering cross section

$$\frac{d\sigma(q)}{d\Omega} = I_{ves} + I_{mic} = \Delta\rho_m{}^2[f_{ves}4\pi\langle A\rangle_w\Gamma_m P_{bil}(q)\langle V^2 P_{shell}(q)\rangle + (1 - f_{ves})M_{mic}P_{ellips}(q)P_{rod}(q)] \quad (13)$$

which is written as a sum of the contributions from vesicles and micelles, respectively, and where the mass fraction of vesicles is denoted f_{ves}, assuming an identical composition in micelles and bilayers. The micelles are assumed to be shaped as rods with an elliptical cross section in accordance with what we found in samples containing only micelles.[14,15] The corresponding form factor was separated into one factor valid for infinitely thin rods of length L[35]

$$P_{rod}(q,L) = 2\mathrm{Si}(qL) - \frac{4\sin^2(qL/2)}{(qL)^2} \quad (14)$$

where

$$\mathrm{Si}(x) = \int_0^x \frac{\sin t}{t}\,dt \quad (15)$$

and one factor that accounts for an elliptical cross section with half axes a and b

$$P_{ellips}(q) = \frac{2}{\pi}\int_0^{\pi/2}\left[\frac{2B_1(qr(a,b,\phi))}{qr(a,b,\phi)}\right]^2 d\phi \quad (16)$$

where $r(a,b,\phi) = [a^2\sin^2\phi + b^2\cos^2\phi]^{1/2}$ and $B_1(x)$ is the Bessel function of first order. In order to avoid a far too complicated model, we have assumed the micelles to be monodisperse rather than polydisperse.

In the absence of added salt, we found the coexistence of 95 wt % micelles and 5% vesicles at [$X = 0.15$, $c^{tot}_{surf} = 0.50$ wt %], and at [$X = 0.75$, $c^{tot}_{surf} = 0.50$ wt %], the fraction of vesicles was seen to be 7.5%. The fraction of vesicles increased from less than 1% at $X = 0.25$ via 75% at $X = 0.30$ to 87% at $X = 0.32$ at $c^{tot}_{surf} = 1.0$ wt %. We also observed that very small amounts (<1%) of larger particles, assumed to be either vesicles or lamellar sheets, coexist with micelles at [$X = 0.70$, $c^{tot}_{surf} =$ 1.0 and 5.0 wt %] and at [$X = 0.85$, $c^{tot}_{surf} = 0.25$ wt %].

In the 0.1 M NaBr solutions, we observed that 84% vesicles coexist with micelles at [$X = 0.85$, $c^{tot}_{surf} = 0.05$ wt %]. This sample was also measured with SLS, enabling us to determine the full size distribution of the vesicles coexisting with micelles

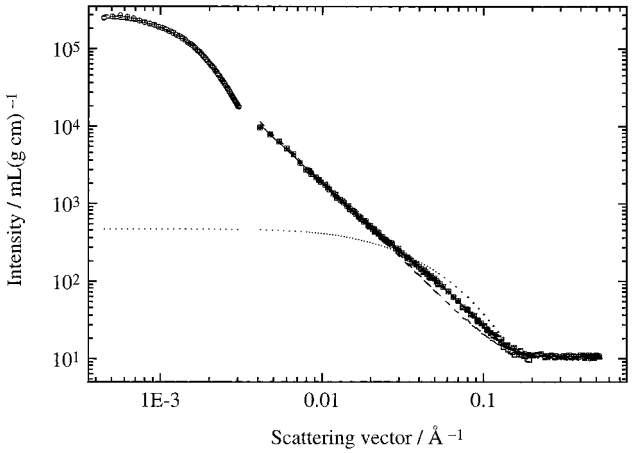

Figure 7. Normalized scattering intensity as a function of scattering vector q for a sample with surfactant molar ratio [SDS]:[DTAB] = 20:80 at an overall surfactant concentration of 0.05 wt % in 0.1 M NaBr. The squared individual symbols represent SANS data obtained with different combinations of neutron wavelength and sample detector distance at Risø, and the circular symbols represent SLS data. The solid lines represent the results from a fit with a model for coexisting polydisperse unilamellar vesicles and monodisperse rigid rods of length L and an elliptical cross section with half axes a and b. A structure factor was neither used for the micelles nor the vesicles in the model. The average radius $\langle R \rangle$ of the vesicles is 674 Å, the relative standard deviation $\sigma_R/\langle R \rangle = 0.44$, and half the bilayer thickness $\xi = 14.6$ Å. The length of the micelles is $L = 82.1$ Å, and the cross-sectional dimensions $a = 14.8$ Å and $b = 28.0$ Å. The mass fraction of vesicles equals 0.84, and the agreement of the fits as measured by χ^2 is 1.6. The dashed line represents a fit with a model for only polydisperse vesicles and the dotted line a model for only monodisperse tablet-shaped micelles.

[cf. Figure 7]. This was the only sample measured with SLS that could be fitted without using a structure factor for sticky hard spheres.

The appearance of the data obtained at ILL (stored 5−10 h at 40 °C before being measured) for the samples $X = 0.85$ at $c_{surf}^{tot} = 0.025$ and 0.05 wt % in brine is very different from that obtained at Risø and ETH (stored 20−25 h before being measured), indicating that the equilibrium processes are rather slow for these very diluted samples where both micelles and vesicles coexist (compare the rapid equilibration in the more concentrated sample containing only vesicles described above). Coexistence of micelles and vesicles at $X = 0.85$ were found in both samples ($c_{surf}^{tot} = 0.025$ and 0.05 wt %) measured at ILL as well as in the sample with $c_{surf}^{tot} = 0.05$ wt % measured at Risø, whereas only vesicles could be found in the samples where $c_{surf}^{tot} = 0.025$, 0.03, and 0.04 wt %, respectively, measured at Risø. However, since latter samples were not measured with SLS, we have not been able to determine the size distributions of the corresponding vesicles.

Conclusions

We have, using small-angle neutron and static light scattering, investigated the various microstructures formed in aqueous mixtures of an anionic (SDS) and a cationic surfactant (DTAB) in the absence of added salt as well as in brine (0.1 M NaBr) at 40 °C. The two main structures found are, on one hand, micelles[14,15] and, on the other hand, various kinds of bilayers including geometrically closed vesicles. The scattering data were analyzed by means of fitting to various models for conceivable surfactant aggregate structures. The risk for ambiguities in the model fit procedure, i.e., the risk that several conceivable models may fit the data equally well, was minimized as data with a wide range of scattering vectors were measured including SLS data where necessary.

Various bilayer structures form in mixtures of SDS and DTAB at sufficiently low surface charge densities, i.e., at sufficiently low mole fractions of the surfactant in excess in the bilayers. We have fitted our SANS data with a paracrystal lamellar model with respect to bilayer thickness, average layer distance, variance in the layer distance distribution, and number of layers. The number of layers of the aggregates formed in the most diluted samples in the absence of added salt was rather small ($1 < N_L < 3$), indicating the formation of unilamellar and some kind of oligolamellar vesicles. At higher surfactant concentrations, N_L is seen to rapidly approach infinity and we conclude that, at compositions where micelles do not form, unfavorable interactions between the comparatively voluminous vesicles cause a transition to stacks of lamellar sheets when the overall surfactant concentration is raised above a certain limit. Close to equimolar composition, beyond about $X = 0.40$ and 0.60, as well as in the most diluted samples, an increasing amount of a precipitate forms.

As NaBr was added to the solutions to give a concentration of 0.1 M, the vesicles were clearly destabilized and either micelles or lamellar sheets form instead. The formation of micelles in brine at compositions where vesicles predominate in the absence of added salt can be rationalized as a consequence of the transition of free monomers into the aggregates as the chemical potential of the surfactant in excess is lowered upon addition of salt. The formation of lamellar sheets is most likely due to an increase in the bilayer bending work with increasing electrolyte concentration.

Static light scattering data from samples containing only vesicles could only be analyzed by means of assuming a significant attraction between the vesicles, resulting in the formation of clusters. From our scattering data, it is, however, difficult to distinguish a model of attracting unilamellar vesicles forming clusters from one for oligolamellar vesicles where smaller aggregates are enclosed by larger ones. The number of layers (N_L) in the paracrystal lamellar model would be related to the number of aggregates included in the cluster rather than the number of bilayers in an oligolamellar vesicle. There is also a rather large correlation between the relative standard deviation of the layer distance ($\sigma_D/\langle D \rangle$) and the number of layers in a single cluster (N_L), resulting in comparatively large estimated errors for these parameters.

The vesicles form immediately as a sample containing micelles is diluted below the micelle-to-vesicle transition limit [cf. Figure 1], and they appear to be equilibrated with respect to internal properties (bilayer thickness, size, and polydispersity) well before 24 h at 40 °C. However, the process of cluster formation, the information of which is contained in the SLS data at lower q values, appears to be slower than the formation of the vesicles themselves, and the corresponding equilibrium time appears to be of the order of days.

It has proved to be difficult for us to determine the polydispersity of the vesicles reliably since the large structure factor effects present may slightly affect the quantitative result of $\sigma_R/\langle R \rangle$ obtained from our fits. Nor is it possible to reduce the influence of the structure factor by simply diluting the samples, as the large free monomer effects cause a dramatic increase in size of the observed bilayer structures.

Acknowledgment. M. B was supported by a Marie Curie Fellowship from the Training and Mobility of the Researches (TMR) Programme of the European Union.

References and Notes

(1) Kamenka, N.; Chorro, M.; Talmon, Y.; Zana, R. *Colloids Surf.* **1992**, *67*, 213.
(2) Kaler, E. W.; Herrington, K. L.; Murthy, A. K.; Zasadzinski, J. A. N. *J. Phys. Chem.* **1992**, *96*, 6698.
(3) Marques, E.; Khan, A.; Miguel, M.G.; Lindman, B. *J. Phys. Chem.* **1993**, *97*, 4729.
(4) Jaeger, D. A.; Brown, E. L. G. *Langmuir* **1996**, *12*, 1976.
(5) Talhout, R.; Engberts, J. B. F. N. *Langmuir* **1997**, *13*, 5001.
(6) Marques, E. F; Regev, O.; Khan, A.; da Graça Miguel, M.; Lindman, B. *J. Phys. Chem. B* **1998**, *102*, 6746.
(7) Helfrich, W. *Naturforsch.* **1973**, *28c*, 109.
(8) Bergström, M. *Prog. Colloid Polym. Sci.* **1997**, *105*, 214.
(9) Bergström, M.; Eriksson, J. C. *Langmuir* **1996**, *12*, 624.
(10) Safran, S. A.; Pincus, P.; Andelman, D.; Mackintosh, F. C. *Phys. Rev. A* **1991**, *43*, 1071.
(11) Bergström, M.; Eriksson, J. C. *Langmuir* **1998**, *14*, 288.
(12) Morse, D. C.; Milner, S. T. *Phys. Rev. E* **1995**, *52*, 5918.
(13) Bergström, M.; Pedersen, J. S. *Langmuir* **1998**, *14*, 3754.
(14) Bergström, M.; Pedersen, J. S. *Langmuir* **1999**, *15*, 2250.
(15) Bergström, M.; Pedersen, J. S. *J. Phys. Chem. B* **1999**, *103*, 8502.
(16) Villeneuve, M.; Kaneshina, S.; Imae, T.; Aratono, M. *Langmuir* **1999**, *15*, 2029.
(17) Pedersen, J. S. *J. Phys. IV (Paris) Collect. C8* **1993**, *3*, 491.
(18) May, R. P.; Thomas, M. A New Low-Q- Scattering Instrument at the Second Cold source of the ILL. ILL Technical Report 86MA07T, Institute Laue-Langevin, Grenöble, France, 1986.
(19) Cotton, J. P. In *Neutron, X-Ray and Light Scattering: Introduction to an Investigative Tool For Colloidal and Polymeric Systems*; Lindner, P., Zemb, T., Eds.; North-Holland: Amsterdam, 1991.
(20) Wignall, G. D.; Bates, F. S. *J. Appl. Crystallogr.* **1986**, *20*, 28.
(21) Chevalier, Y.; Zemb, T. *Rep. Prog. Phys.* **1990**, *53*, 279.
(22) Pedersen, J. S.; Posselt, D.; Mortensen, K. *J. Appl. Crystallogr.* **1990**, *23*, 321.
(23) Bevington, B. R. *Data Reduction and Error Analysis for Physical Sciences*; McGraw-Hill: New York, 1969.
(24) Pedersen, J. S. *Adv. Colloid Interface Sci.* **1997**, *70*, 171.
(25) Jerke, G.; Pedersen, J. S.; Egelhaaf, S. U.; Schurtenberger, P. *Phys. Rev. E* **1997**, *56*, 5772.
(26) Schurtenberger, P.; Augusteyn, R. C. *Biopolymers* **1991**, *31*, 1229.
(27) Guinier, A. *X-Ray Diffraction*; W. H. Freeman and Co: San Francisco.
(28) Pedersen, J. S.; Vyskocil, P.; Schönfeld, B.; Kostorz, G. *J. Appl. Crystallogr.* **1997**, *30*, 975.
(29) Gruen, D. W. R. *J. Phys. Chem.* **1985**, *89*, 153.
(30) Bergström, M. *Langmuir* **1996**, *12*, 2454.
(31) Kotlarchyk, M.; Chen, S. H. *J. Chem. Phys.* **1983**, *79*, 2461.
(32) Baxter, R. J. *J. Chem. Phys.* **1968**, *49*, 2770.
(33) Menon, S. V. G.; Manohar, C.; Srinivasa Rao, K. *J. Chem. Phys.* **1991**, *95*, 9186.
(34) Israelachvili, J. N. *Intermolecular and surface forces;* 2nd ed.; Academic Press: London, 1991; Chapters 16 and 17.
(35) Neugebauer, T. *Ann. Phys. Leipzig* **1943**, *42*, 509.